J Therm Anal Calorim (2015) 121:589–595
DOI 10.1007/s10973-015-4581-5

Calorimetry study of the precipitation in an Al7075-graphite composite fabricated by mechanical alloying and hot extrusion

K. A. Leyva-González · R. Deaquino-Lara · D. Pourjafari · R. Martínez-Sánchez · M. A. L. Hernandez-Rodriguez · E. García-Sánchez

Received: 8 September 2014 / Accepted: 14 February 2015 / Published online: 28 March 2015

Abstract Differential scanning calorimetry (DSC) technique was used to study the effect of adding graphite particles as well as the effect of different amounts of zinc over the precipitation sequence in a 7075 aluminum alloy. Recent works have shown that the graphite can be used to enhance the mechanical properties of the 7xxx aluminum alloys. According to the DSC results, the peaks were identified as dissolution of Guinier–Preston zones, precipitation of η', dissolution of η', precipitation of η and dissolution of η. These transformations were studied by using heating rates of 5, 10 and 20 °C min^{-1} at different natural aging times (1, 5.5 h and 5 days). The Kissinger's method was applied to calculate the activation energies from peak temperatures. Results showed that the greater heating rate is, the greater amount of energy is required; as well as the greater natural aging time, the smaller energy to generate the precipitation in this composite. An important change in the energy requirement for phase transformations, mainly for the η' phase, was generated by the addition of graphite particles (C). Vickers microhardness was also used as a complementary technique to determine the effect of both graphite and zinc contents over the mechanical properties. The results showed that C promotes an important increase in microhardness in a short time compared with a conventional 7075 alloy. In addition, the mechanical properties of the composite increased in direct relation to the addition of graphite. These particles also decrease the amount of energy required to generate the phases.

Keywords 7075 · Precipitation · Natural aging · Aluminum alloy

K. A. Leyva-González · M. A. L. Hernandez-Rodriguez · E. García-Sánchez (✉)
Facultad de Ingeniería Mécanica y Eléctrica, Universidad Autónoma de Nuevo León, 66450 San Nicolás de los Garza, Nuevo Leon, Mexico
e-mail: egs7710@gmail.com

R. Deaquino-Lara
Centro de Investigación y de Estudios Avanzados del IPN (CINVESTAV), Unidad Saltillo Carretera Saltillo-Monterrey km 13.5, C.P. 25000 Ramos Arizpe, Coahuila, Mexico

D. Pourjafari
Departamento de Física Aplicada, Centro de Investigación y de Estudios Avanzados del IPN, 97310 Mérida, Yucatán, Mexico

R. Martínez-Sánchez
Laboratorio Nacional de Nanotecnología, Centro de Investigación en Materiales Avanzados (CIMAV), Miguel de Cervantes No. 120, C.P. 31109 Chihuahua, Chihuahua, Mexico

Introduction

Among all aluminum alloys, the 7xxx series have received special attention because they provide the highest strength. These series have been widely used as a matrix of several composites. The aluminum matrix composites have been used in many different applications such are aerospace and automotive structures. There are some strengthening agents as oxides, carbides and nitrides, which are typically used in these composites. In recent surveys it was found that graphite particles could also be applied as a reinforcing agent in aluminum composites improving the mechanical properties of the material [1, 2].

During the natural aging of the 7075 alloy, several metastable precipitates may be formed and the final properties of the composite dependent of the type of

precipitates. However, these phenomena have not been systematically studied in an Al7075-C composite manufactured by mechanical alloying technique (MA). This technique (MA) is frequently used for manufacturing these types of materials; MA provides important and specific characteristics as large amount of crystal defects inside of the particles, as a consequence of severe plastic deformation. This crystal defects represents a great amount of internal stored energy, which is the driving force for recrystallization and second phases precipitates formation during the post-processing.

Calorimetric techniques have been useful to study the precipitation phenomena in some materials such as aluminum [3, 4], magnesium [5], copper [6], metal matrix composites [7], and others. Differential scanning calorimetry (DSC) is a convenient method used to study thermal events such as phase transformations [8], the kinetics reaction and activation energies related to these transformations [5], effect of alloy elements [9]. This research is focused on the study of the graphite effect on the precipitation sequence in the Al7075-C composite obtained by mechanical alloying and hot extrusion.

Experimental

In this study, twelve cylindrical specimens of 7075 aluminum alloy-graphite with different compositions were studied; the length and diameter of these bars were 25 and 1 cm respectively. These specimens were obtained by powder metallurgy using high energy milling processes and hot extrusion, starting from pure elements in appropriate proportions, the amount of each element added to form the composite correspond with the chemical composition given in Table 1. Details of the processing parameters of these composites were reported previously [2].

A total of 12 samples with a height of 1 cm were taken from the cross-section of each cylindrical specimen. All the samples were first mechanically roughened and polished with alumina (1 μm) in a Struers Labopol-1. Then, Vickers microhardness tests were performed using a Shimadzu HMV-2TE microhardness tester with a load of 1.96 N for 15 s. Finally, average microhardness values were obtained from 10 indentations on each sample.

A set of four samples (S1, S2, S3 and S4) received a heat treatment in a conventional furnace Thermolyne F6010: solubilization at 550 °C for 2 h, water quenching at room temperature (25 °C) followed for a natural aging (1, 5 h, 5, 10 and 15 days) in order to study its effect on the mechanical properties.

Finally, small disks with a thickness near to 1 and 6 mm diameter were taken of the set of four samples. They were roughened, mechanically polished and electropolished [10] in a D-612 filtered DC power supply by using a solution of 2-Butoxyethanol, perchloric acid (60 %), ethanol, and distilled water in 2, 8, 30 and 60 vol% respectively during about 5 min at 7 °C, with 8 V. This was performed to obtain a flat and micro-deformation free surface, the diameter of each sample was almost the same as the pans improving the thermal contact. All the samples presented a mass of 0.023 g approximately (Ohaus Explorer analytical balance). The DSC analyses were performed in a DSC 404 F3 Netzsch heating up to 550 °C in an Ar atmosphere, measurements with heating rates of 5, 10, 20 °C min^{-1} were performed. Aluminum pans were used for all tests and the baseline was obtained using empty aluminum pans as reference.

Results and discussion

Vickers microhardness

The effect of zinc over microhardness for samples with different graphite content (0.0, 0.5, 1.0 and 1.5 mass%) is presented in Fig. 1.

According to Fig. 1 there is a small variation in the microhardness values for samples with 0 mass% and 0.5 graphite (C) mass%. But, the variation is higher if the zinc content increases for samples with 1 C mass% and 1.5 C mass%. All samples showed the highest microhardness values increasing graphite content. This influence is more evident in samples with 4.1 Zn mass%. For samples without graphite, the greatest value of microhardness was observed with the lowest zinc content.

The results in Fig. 2 of the tests for different natural aging times (1, 5 h, 5, 10 and 15 days), exhibited a clear tendency: the microhardness increases with the aging time.

Table 1 Composition of the composites/mass%

Element/mass%	Sample											
	S1	S1.1	S1.2	S2	S2.1	S2.2	S2.3	S2.4	S3	S3.1	S3.2	S4
C	0	0.5	1	1.5	0	0.5	1	1.5	0	0.5	1	1.5
Zn	5.1	5.1	5.1	5.1	4.1	4.1	4.1	4.1	3.1	3.1	3.1	3.1
	2.5 Mg, 1.6 Cu, 0.3 Fe, 0.2 Mn, Al Balance											

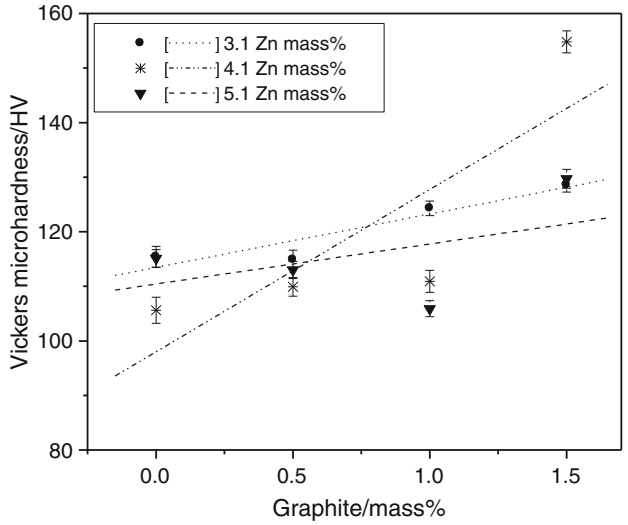

Fig. 1 Graphite effect on Vickers microhardness

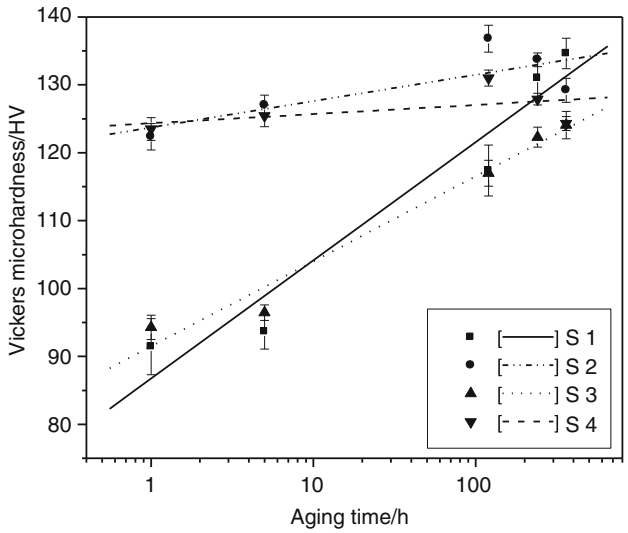

Fig. 2 Natural aging effect on Vickers microhardness

This behavior is observed in other aluminum alloys [3, 4]. This effect is higher for samples without graphite. It is expected that all samples reach a maximum microhardness value/HV and then, for longer aging times these values will be stabilized. These results show the contribution of graphite for hardening of the composite. The slope of the curves can be associated with Zn precipitates formation.

Finally, when this composite was naturally aged, a maximum microhardness (~135 HV) was reached at 15 days. Comparing this value with the microhardness from another 7075 alloy naturally aged without reinforcing the alloy reaches a value near to 150 HV after 45 days [11]. In general graphite particles promote a greater microhardness in a shorter time compared with a 7075 alloy.

DSC results

The 7075 alloy shows a very wide solid solution range and almost all Zn, Mg and Cu can be remain into the supersatured solid solution (SSS) during quenching, these alloys after quenching show natural aging associated with the start of sequence of precipitation, at this moment, the alloying elements are expulsed of the Al crystalline structure forming the first clusters [12].

The sequence of precipitation for 7xxx aluminum series has been proposed according to (1):

$$\text{GP zones}(\text{MgZn}) \rightarrow \eta' \text{ or } T' \rightarrow \eta(\text{MgZn}_2) \text{ or } T(\text{Al}_2\text{Zn}_3\text{Mg}_3) \quad (1)$$

However this sequence will depend of the chemical composition, and mainly on the Mg:Zn ratio in the alloy [12, 13]. The formation and evolution of precipitates developed during aging treatments were studied by DSC. The composition effect, the heating rate and the natural aging time effect in the energetic characteristics and precipitation in the composite were studied.

After each aging time, the samples S1, S2, S3 and S4 (Table 1) were studied immediately by DSC. Figure 3 shows the results of the thermal events in the samples after 5.5 h of natural aging time under a heating rate of 10 °C min^{-1}.

All thermal events were identified according to the temperatures at which the peaks were located in the curves. According to the location of the endothermic peak A and other studies this region corresponds to the dissolution of Guinier–Preston zones (GP) [4, 14–17]. The GP solvus temperature is sensitive and increases with the Zn and Mg content, region A shows this shift in the solvus temperature

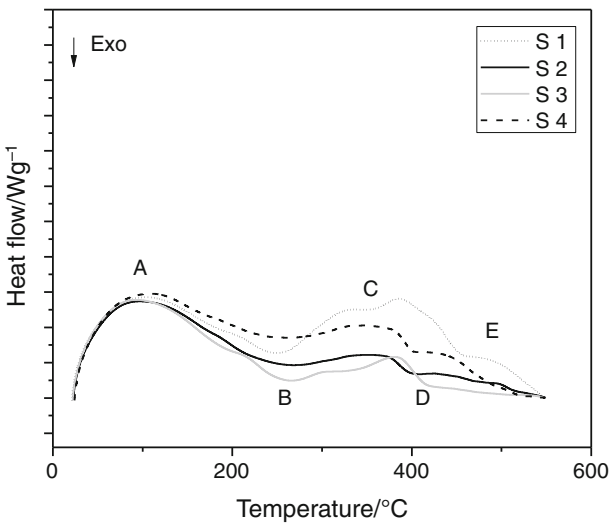

Fig. 3 Curves of the samples 1, 2, 3 and 4, after 5.5 h of natural aging at 10 °C min^{-1}

for samples S1 and S3. The region B could be associated with the two phases. However, if the Mg:Zn ratio in the alloy (7xxx) is between 0.14 and 0.4, then coherent η phase could be the final phase, and if the Mg:Zn ratio is between 0.5 and 6, then the sequence could finish with the precipitation of T phase [12]. Some authors [4, 18–20] correlate this peak to the precipitation of η', T' or both depending on several conditions. In this work the Mg:Zn ratio is between 0.49 and 0.8 corresponding to the maximum amount of Zn (5.1 mass%) and to the minimum Zn content (3.1 mass%), respectively. However, other elements also have an important effect on the transformation temperatures [21], for example, the copper levels below of 1 % mass do not affect the precipitation sequence but when the alloy has high copper content (in this study 1.6 mass%) there is a contribution to the hardening of material, due to copper atoms diffuse into the GP zones and change the composition of the η phase or forming another phase called S' phase (Al_2CuMg) [12]. This is the reason why it was not considered convenient only to use the Mg:Zn ratio to determine the final phase. Furthermore, these phases usually appear in a similar range of temperatures. We analyze the results of similar researches based on more precise techniques such as TEM for identifying this peak. Most authors [18, 22–24] agree that the final phase corresponds to η phase, therefore, the intermediate phase is η'. Due to the accuracy of this technique, ensuring that η phase formation corresponds to peak B, is feasible. The endothermic peak C corresponds to η' phase dissolution [4, 18, 24]; the samples S1 and S3 showed a "double" peak in this area, this could be explained as the overlap of the dissolution of η' phase and the precipitation of η phase, these are not observed in the curves S2 and S4 corresponding to samples with 1.5 C mass%. The exothermic peak D corresponds to the precipitation of η phase [4, 12, 18, 19]. The peak E was associated to the dissolution of η phase [3, 19].

The effect of graphite on GP zones dissolution, peak A, can be seen in Fig. 3. The maximum dissolution is reached between 93 and 108 °C, depending on the composition of the sample, this variation was considered as significant. In Fig. 3 this peak occurs at similar temperatures in samples S1 and S2, 102 and 96 °C respectively. Also the heat required to dissolve this phase was similar in magnitude for samples, 0.143 and 0.137 W g^{-1}. The sample with graphite (S2) is slightly less endothermic affecting the phase change in this area. This can be considered as graphite promotes the GP zones dissolution when samples have 5.1 Zn mass%. The η' phase (peak B) precipitated easily in the samples S1 and S4. This is interpreted as a lower energy requirement for the phase change, at which zinc has an important influence. According to the peak C of the samples S2 and S4, η' phase dissolution occurs at lower temperatures, this reduction was associated with the graphite content.

It is difficult to find the peaks D and E in the curves, this can be explained as the dissolution and precipitation energies under those conditions are very similar, which generates these peaks do not be significant in the Fig. 3.

Heating rate effect on precipitation sequence

The obtained DSC curves and the phase transformation temperatures were used to calculate the activation energies, which change with the temperature [21]. The activation energies were calculated using the Kissinger's method [5, 25], which depends on the absorbed or released heat by each transition at different heating rates (5, 10 and 20 °C min^{-1}). The results are presented in Fig. 4. These samples were naturally aged during 5.5 h. The precipitation and dissolution temperatures are shown in Table 2. The peaks were associated with: peak A: Guinier–Preston zones dissolution [4, 14–17] (GP), exothermic peak B: η' precipitation [18, 22–24, 26, 27]. The "double peak" which

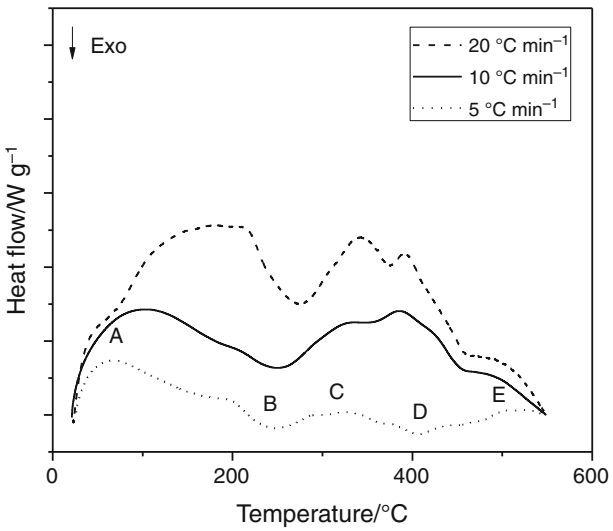

Fig. 4 Curves of the sample 1 after 5.5 h aging for three different heating rates: 5, 10 and 20 °C min^{-1}

Table 2 Precipitation and dissolution phase temperatures for the sample S1 under different heating rates

Heating rate/°C min^{-1}	Temperature/°C				
	Peak A	Peak B	Peak C		Peak D
			Peak I	Peak II	
20	184	275	343	391	–
10	103	250	317	386	–
5	66	248	285	–	407

is present in the endothermic peak C represents the overlap of the η' phase dissolution [4, 9, 12, 20] and η phase precipitation. Finally, the peak D is associated to the η phase precipitation [4, 12, 18, 19].

The activation energy was calculated using the Kissinger's method (2):

$$\ln\left(\frac{T^2}{\beta}\right) = \frac{E}{RT} + C \quad (2)$$

Symbols	Description
T	Peak temperature/°C
β	Heating rate/°C min^{-1}
E	Activation energy/KJ mol^{-1}
R	Universal constant used for ideal gases/8.314 J mol^{-1} K^{-1}
C	Constant

Kissinger's equation has the form of an Arrhenius' equation. The slope of the resulting line will have a value of ER^{-1}; we can determine the activation energy (E) from this.

Dimensional analysis was performed and the resulting activation energies were: 8.4 kJ mol^{-1} (peak A), 90.4 kJ mol^{-1} (peak B) and 99.8 kJ mol^{-1} (peak I–C). This is the minimum required energy to start the precipitation or dissolution phases.

By comparing the peak A (Fig. 4) of the three heating rates, can be seen that it requires a greater amount of energy to dissolve GP zones when the analysis is performed at 20 °C min^{-1}; it represents higher energy consumption. Furthermore, the dissolution takes place at higher temperatures than the other rates. The peak B is more intense at 20 °C min^{-1}, which indicates that at lower heating rates, the precipitation takes place in a wider range of temperatures. In general, these results suggest that as the heating rate increases, the energy released in this phase will also increase. The absorbed energy to dissolve η' phase at 20 °C min^{-1} is higher than the other rates; therefore it is easier to dissolve the phase corresponding to peak C at lower rates. The precipitation of η (peak D) is almost no appreciable at 10 and 20 °C min^{-1}; this phase occurs at lower temperatures when the sample is analyzed at 5 °C min^{-1}. The peak E is endothermic, although it is only perceived at low rates. The rate of 5 °C min^{-1} allows phase dissolution to absorb less energy and the precipitates formation to releases less energy. In addition to these aging conditions and composition, η phase dissolution is visible only at low rates.

The activation energies were calculated for all samples, the results are shown in Table 3. These values are small when compared to other alloys, we could notice it with

Table 3 Activation energies of the set of four samples studied and other references

Alloy	Activation energy/kJ mol^{-1}			
	GP zones dissolution	η' precipitation	η' dissolution	References
7075 alloy				
1	8.4	90.4	99.8	Study
2	7.8	33.6	33.85	
3	8.5	33.24	–	
4	10.3	19.71	101.25	
7017	71.8 ± 10.7	62.1 ± 8.9	–	[3]
7150	33 ± 1.88	–	96.42 ± 8.98	[4]

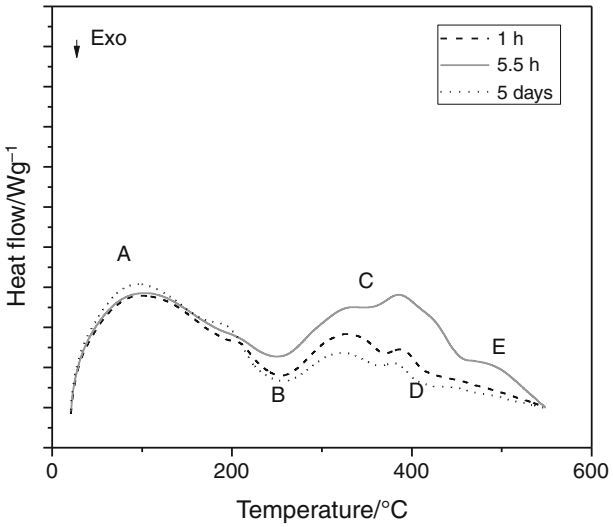

Fig. 5 Curves of the sample 1 after 5.5 h analyzed at 10 °C min^{-1}

comparing 7150 and 7017 alloy in the GP region, this suggests that graphite particles may be acting as a kind of catalyst since the energy required to dissolve those phases is reduced with the amount of graphite increases. The energy to dissolve η' phase for samples S1 and S4 is similar to some references (Table 3), this could mean that this phase dissolution is not so significantly influenced by the composition.

Effect of natural aging time on the precipitation sequence

In this section the aging time effect on the precipitation in the composite was discussed. The results are shown in Fig. 5. The ideal time for the sample S1, coincides with 5 days of natural aging. This time will benefit the precipitation sequence.

Conclusions

According to the results, the addition of graphite particles in the 7075 alloy (Al–Zn–Mg–Cu) increases the hardness material. The graphite particles increase strength as well as decrease the mobility of dislocations in the metal matrix, causing strengthening due to the fine dispersion of particles.

The graphite particles promote a greater microhardnesss in a shorter time during natural aging of the composite compared with a 7075 alloy.

The sequence of precipitation of the composite under the studied conditions was determinate as: GP zones dissolution, η' precipitation, η' dissolution, η precipitation and η phase dissolution.

For the analyzed graphite compositions the sequence of precipitation is not affected in this composite. In samples without graphite, the zinc contributes to a lower energy requirement and, when the samples contain graphite, a smaller amount of zinc contributes to a lower energy requirement.

Increasing the heating rate, the amount of energy needed to generate both the precipitation and dissolution phases also is major.

The temperatures of phase transitions for all samples were affected by the amount of graphite; graphite promotes the η phase precipitation at lower temperatures compared with the temperatures of the samples without graphite.

The activation energies obtained by Kissinger's method were analyzed and it was found that graphite particles may act as a kind of catalyst, where a smaller amount of energy is required to dissolve the phases, compared to other alloys.

References

1. Estrada-Guel I, Carreño-Gallardo C, Mendoza-Ruiz DC, Miki-Yoshida M, Rocha-Rangel E, Martínez-Sánchez R. Graphite nanoparticle dispersion in 7075 aluminum alloy by means of mechanical alloying. J Alloys Compd. 2009;483(1–2):173–7. doi:10.1016/j.jallcom.2008.07.190.
2. Deaquino-Lara R, Estrada-Guel I, Hinojosa-Ruiz G, Flores-Campos R, Herrera-Ramírez JM, Martínez-Sánchez R. Synthesis of aluminum alloy 7075-graphite composites by milling processes and hot extrusion. J Alloys Compd. 2011;509(Suppl 1(0)):S284–9.
3. Ghosh KS, Kumar AK, Mohan MK. Calorimetric studies and kinetic parameters of solid state reactions in 7017 Al–Zn–Mg alloy. Trans Indian Inst Met. 2008;61(6):487–96. doi:10.1007/s12666-008-0056-8.
4. Ghosh KS, Gao N. Determination of kinetic parameters from calorimetric study of solid state reactions in 7150 Al–Zn–Mg alloy. Trans Nonferrous Met Soc China. 2011;21(6):1199–209. doi:10.1016/S1003-6326(11)60843-1.
5. Barrena MI, Gómez de Salazar JM, Pascual L, Soria A. Determination of the kinetic parameters in magnesium alloy using TEM and DSC techniques. J Therm Anal Calorim. 2013;113(2):713–20. doi:10.1007/s10973-012-2791-7.
6. Saud S, Hamzah E, Abubakar T, Bakhsheshi-Rad HR. Thermal aging behavior in Cu–Al–Ni–xCo shape memory alloys. J Therm Anal Calorim. 2015;119(2):1273–84. doi:10.1007/s10973-014-4265-6.
7. Buytoz S, Dagdelen F, Islak S, Kok M, Kir D, Ercan E. Effect of the TiC content on microstructure and thermal properties of Cu–TiC composites prepared by powder metallurgy. J Therm Anal Calorim. 2014;117(3):1277–83. doi:10.1007/s10973-014-3900-6.
8. Deris L, Sharafi S, Akbari GH. Effect of milling speed on mechanical activation of Al/ZrO_2/H_3BO_3 system to prepare Al_2O_3–ZrB_2 composite powder. J Therm Anal Calorim. 2014;115(1):401–7. doi:10.1007/s10973-013-3235-8.
9. Klančnik G, Medved J, Nagode A, Novak G, Steiner Petrovič D. Influence of Mn on the solidification of Fe–Si–Al alloy for non-oriented electrical steel. J Therm Anal Calorim. 2014;116(1):295–302. doi:10.1007/s10973-013-3536-y.
10. Poorganji B, Sepehrband P, Jin H, Esmaeili S. Effect of cold work and non-isothermal annealing on the recrystallization behavior and texture evolution of a precipitation-hardenable aluminum alloy. Scr Mater. 2010;63(12):1157–60. doi:10.1016/j.scriptamat.2010.08.014.
11. Deschamps A, De Geuser F, Horita Z, Lee S, Renou G. Precipitation kinetics in a severely plastically deformed 7075 aluminium alloy. Acta Mater. 2014;66:105–17. doi:10.1016/j.actamat.2013.11.071.
12. Totten GE, MacKenzie DS. Handbook of aluminum: physical metallurgy and processes. New York: Marcel Dekker; 2003.
13. García C, Louis E. Thermal analysis of aluminum alloys. In: Mackenzie DS, Totten GE, editors. Analytical characterization of aluminum, steel, and superalloys. New York: CRC Press, Taylor & Francis; 2006.
14. Chen SP, Mussert KM, van der Zwaag S. Precipitation kinetics in Al6061 and in an Al6061-alumina particle composite. J Mater Sci. 1998;33(18):4477–83. doi:10.1023/a:1004414413800.
15. Gómez De Salazar JM, Barrena MI. The influence of Si and Mg rich phases on the mechanical properties of 6061 Al-matrix composites reinforced with Al_2O_3. J Mater Sci. 2002;37(8):1497–502. doi:10.1023/a:1014967324577.
16. Min Z, Gaohui W, Longtao J. Aging behavior and precipitation kinetics of SiCp/6061AI composites. J Mater Sci. 2004;39(5):1759–63. doi:10.1023/B:JMSC.0000016181.46467.0e.
17. Sheu C-Y, Lin S-J. Ageing behaviour of SiCp-reinforced AA 7075 composites. J Mater Sci. 1997;32(7):1741–7. doi:10.1023/a:1018576000575.
18. Li XM, Starink MJ. DSC study on phase transitions and their correlation with properties of overaged Al–Zn–Mg–Cu alloys. J Mater Eng Perform. 2012;21(6):977–84. doi:10.1007/s11665-011-9973-5.
19. Li XM, Starink M. Effect of compositional variations on characteristics of coarse intermetallic particles in overaged 7000 aluminium alloys. Mater Sci Technol. 2001;17(11):1324–8.
20. Papazian J. Calorimetric studies of precipitation and dissolution kinetics in aluminum alloys 2219 and 7075. MTA. 1982;13(5):761–9. doi:10.1007/bf02642389.
21. Karagoz Z, Canbay CA. Relationship between transformation temperatures and alloying elements in Cu–Al–Ni shape memory alloys. J Therm Anal Calorim. 2013;114(3):1069–74. doi:10.1007/s10973-013-3145-9.
22. Adler P, DeIasi R. Calorimetric studies of 7000 series aluminum alloys: II. Comparison of 7075, 7050 and RX720 alloys. MTA. 1977;8(7):1185–90. doi:10.1007/bf02667404.

23. Fang X, Song M, Li K, Du Y, Zhao D, Jiang C, et al. Effects of Cu and Al on the crystal structure and composition of η (MgZn2) phase in over-aged Al–Zn–Mg–Cu alloys. J Mater Sci. 2012;47(14):5419–27. doi:10.1007/s10853-012-6428-9.
24. Jiang XJ, Tafto J, Noble B, Holme B, Waterloo G. Differential scanning calorimetry and electron diffraction investigation on low-temperature aging in Al–Zn–Mg alloys. Metall Mater Trans A. 2000;31(2):339–48. doi:10.1007/s11661-000-0269-x.
25. Ovono Ovono D, Guillot I, Massinon D. Determination of the activation energy in a cast aluminium alloy by TEM and DSC. J Alloys Compd. 2007;432(1–2):241–6. doi:10.1016/j.jallcom.2006.05.132.
26. Jiang XJ, Noble B, Hansen V, Tafto J. Influence of zirconium and copper on the early stages of aging in Al–Zn–Mg alloys. Metall Mater Trans A. 2001;32(5):1063–73. doi:10.1007/s11661-001-0117-7.
27. Li X, Xiong B, Zhang Y, Hua C, Wang F, Zhu B, et al. Effect of one-step aging on microstructure and properties of a novel Al–Zn–Mg–Cu–Zr alloy. Sci China Ser E-Technol Sci. 2009;52(1):67–71. doi:10.1007/s11431-008-0277-4.